The 7th International Supercritical CO_2 Power Cycles Symposium
February 21 – 24, 2022, San Antonio, Texas

Paper #115

Gaurav Kumar
Principal Engineer
Convergent Science
New Braunfels, TX
(gaurav.kumar@convergecfd.com)

K.R.V. Manikantachari
Center for Advanced Turbomachinery and Energy Research (CATER),
University of Central Florida,
Orlando, FL
(raghu@ucf.edu)

Scott Drennan
Director of Gas Turbines
Convergent Science
New Braunfels, TX
(scott.drennan@convergecfd.com)

Subith S. Vasu
Center for Advanced Turbomachinery and Energy Research,
University of Central Florida,
Orlando, FL
(subith@ucf.edu)

Scott M. Martin
Eagle Flight Research Center,
Embry-Riddle Aeronautical University,
Daytona Beach, FL
(martis38@erau.edu)

Study of the effect of CO addition in a Direct Fired Oxy-Fuel Combustor for sCO_2 Power Cycles using Direct Detailed Chemistry and Adaptive Mesh Refinement

ABSTRACT

The supercritical power cycle, which employs oxy combustion at very high pressure, is a novel emerging technology which holds a potential for clean energy and meeting the need for growing energy need. Computational Fluid Dynamics (CFD) is poised to play a key role in design and development of this technology due to the increased cost and challenges in experiments due to extremely high pressure (~300bar). A key piece in a robust CFD modeling of sCO_2 combustors is the chemical mechanism governing the combustion reactions. Most mechanisms have not been designed for or validated at such high pressures. It is only recently that the sCO_2 community has started undertaking the effort to create mechanisms from the basics. In the meanwhile, it is therefore imperative to test the existing mechanisms to identify the differences in prediction of flame shape, temperature, and species. The sCO_2 combustors work in a semi-closed loop where exhaust CO_2 is cycled back into the combustion chamber after removal of water and other impurities. It is understood that some CO may make its way back into the combustion chamber along with recycled CO_2. This could pose a problem if a positive feedback loop in CO is established. In this work, we first study two key mechanisms for methane combustion in prediction of flow, flame shape and emission species. Then we undertake a study to investigate the effect of CO addition and to determine if a concept sCO_2 combustor establishes a positive feedback loop which would adversely affect the performance of the combustion system. The concept combustor used for numerical study has been designed at SWRI. The numerical framework uses a direct detailed chemistry solver along with adaptive mesh refinement to capture the flame shape and flow gradients.

INTRODUCTION

The supercritical CO_2 (sCO_2) power cycle is an emerging technology which has the potential to address both environmental concerns and energy demands. The well-known features of this power cycle are: 1) high expected cycle efficiency compared to corresponding HE, AR and steam cycles, 2) compactness of the overall power plant, 3) complete capture of CO_2, and 4) the wide applicability in most power producing applications. Since the power cycle is closed loop and the working fluid is sCO_2, the CO_2 produced by direct-fired, oxy-methane combustion can be recirculated within the same cycle loop. Excess supercritical CO_2 from the cycle can be used for other commercial purposes [1]. A schematic of direct fired sCO_2 cycle is shown in Figure 1. This layout shows that oxygen is separated from air by using an air separation unit (ASU), and methane and oxygen are ignited in the combustion chamber in the presence of sCO_2. Current state-of-art peak operating pressures for sCO_2 combustion are approximately 300 atm [1] and the level of CO_2 dilution in the combustor is more than 95% percent by mass. Here, the presence of sCO_2 at 300 atm shows a different dilution effect on combustion phenomenon compared to N_2 (air-diluted combustion) due to significant differences in thermo-chemical properties. This means that the combustion characteristics could be considerably different in sCO_2 combustion compared to air-diluted cases. At these extreme pressure conditions, experiments are expensive, time consuming, and potentially dangerous. Therefore, modeling would play an important role.

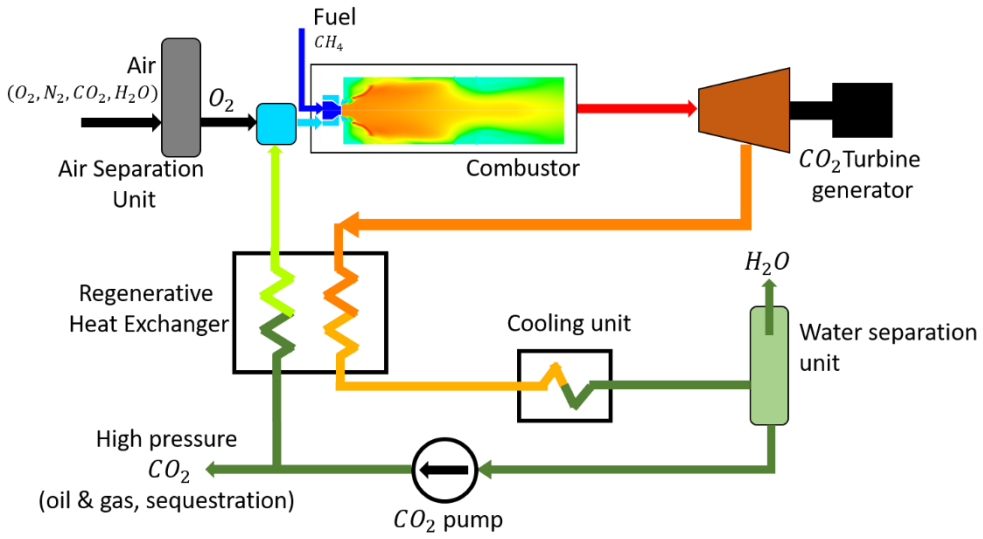

Figure 1: Schematic of Allam cycle which makes the basis for sCO_2 combustors

Managing impurities in the cycle is another foreseen stumbling block for successful operation of sCO_2 combustors. The work in [2] showed that impurities could significantly influence sCO_2 cycle performance. Hence, it is crucial to understand the effect of impurities on sCO_2 combustion. There are several numerical and experimental studies on sCO_2 combustion [3-13]. However, studies related to the effect of impurities on sCO_2 combustion are scant.

Some of the key sources of impurities in sCO_2 combustion are impurities in the fuel, impurities due to inefficiency of air-separation unit before combustor, and impurities due to inefficiency of water separation unit after the heat exchanger. Fuel may also contain traces of H_2S , H_2O, C_2H_6 and C_4H_{10}. Also, an ineffective air-separation unit may not filter Ar and N_2 entirely. Importantly, the water separation unit may not separate CO, H_2O and other minor

combustion products coming from the exhaust stream. As the sCO_2 cycle is operated in a semi-closed loop, these impurities may re-enter the combustion chamber and alter combustor performance. An attempt is made in this work to understand effect of CO impurity on the combustion chamber performance.

METHODS

In this work, the CONVERGE CFD [16] software package is used as the computational framework for RANS finite rate detailed chemistry combustion simulations. CONVERGE is a general purpose CFD code for calculation of three-dimensional, incompressible/compressible, chemically reacting fluid flows with conjugate heat transfer at solid walls in complex geometries with stationary/moving boundaries. CONVERGE solver can handle an arbitrary number of species and chemical reactions, as well as transient liquid sprays, and laminar or turbulent flows. It uses an innovative modified cut-cell cartesian method that eliminates the need for the computational grid to be morphed with the geometry of interest while still precisely representing the true boundary shape. The geometry surface is immersed within a Cartesian block and then cells are trimmed at the intersecting surface. The intersection information is reduced before being stored for each cell. This approach allows for the use of simple orthogonal grids and completely automates the mesh generation process. This section presents a brief overview of the mesh manipulation, numerical algorithms, and physical sub-models used in the current work as these elements all contribute to the grid convergence behavior achieved.

Numerical Algorithms

In the CONVERGE CFD solver, all computed values are collocated at the center of the computational cell. To prevent checker-boarding, the Rhie-Chow [17] algorithm is employed. The conservation equations are solved using the finite volume method. A second order accurate spatial discretization scheme is used for the governing conservation equations and a fully implicit first order accurate time integration scheme.

In the present study a second order accurate spatial discretization scheme is used for the governing conservation equations. In order to maintain stability, time accuracy is set to first order. The transport equations are solved using the Pressure Implicit with Splitting of Operators (PISO) method of Issa [18]. A geometric multigrid solver is used for the pressure solution. A variable time-stepping algorithm is used in the current study. The time-step is automatically calculated each computational cycle based on maximum allowed Courant-Friedrichs-Lewy (CFL) numbers for convection, diffusion and the speed of sound. The calculations in this study are run in parallel on distributed memory machines using the Message Passing Interface (MPI). An automatic domain decomposition technique (using METIS) is employed which allows for efficient load balancing throughout the calculation as the distribution of cells can change significantly due to adaptive mesh refinement. The chemistry calculations are parallelized independent of Navier Stokes solver, which allows for a more balanced computational “load distribution”.

Adaptive Mesh Refinement (AMR)

It is often desirable to add grid resolution locally in critical flow sections of the domain while leaving less critical sections relatively coarse. In the present work, extra grid resolution was added to resolve the complex flow behavior in regions of interest such as near the tiny fuel/air holes and swirler, while leaving the remaining grid relatively coarse to minimize simulation time. It is important to note that fixed embedding is specified in a small volume close to the injector and primary zone (see Figure 2) and is only meant to seed the AMR described below.

In most cases, it is difficult to determine a priori where fixed grid embedding should be added in the flow field. In these cases, Adaptive Mesh Refinement [19,20] can be applied. Ideally, a good AMR algorithm should add embedding where the flow field is most under-resolved or where the sub-grid field is the largest. The current flow solver estimates the magnitude of the sub-grid field of temperature and velocity to determine where embedding should be added or removed. For a scalar, the sub-grid field (ϕ') is defined as the difference between actual (ϕ) and resolved field ($\bar{\phi}$), $\phi' = \phi - \bar{\phi}$. The sub-grid field can also be expressed as an infinite series [21] whose first term (second order term) is used to approximate the sub-grid scale

$$\phi' = -\alpha_{[k]} \frac{\partial^2 \bar{\phi}}{\partial x_k \partial x_k}$$

where, α_k is $(dx_k)^2/24$ for rectangular shaped cell and brackets [.] indicate no summation. The sub-grid expression for scalar is easily generalized for a vector field like velocity. From the expression for sub-grid field, it is evident that AMR is based on the curvature (second derivative) of shear and normal components (of velocity and temperature gradients). The volume mesh is redrawn at every computational time step, according to a boundary/surface definition file. The volume mesh is refined only where necessary, thereby minimizing the total cell count and the run time.

A cell is embedded if the absolute value of the sub-grid is above a user-specified value. Conversely, a cell is "released" (i.e., the embedding is removed) if the absolute value of the sub-grid is below 1/5th of the user-specified value. To limit the number of embedded cells, a maximum overall number of cells can be specified by the user. With this feature, the user can specify the total number of cells desired in the simulation and AMR will determine where to put the embedding to both best resolve the flow field and meet the target number of cells.

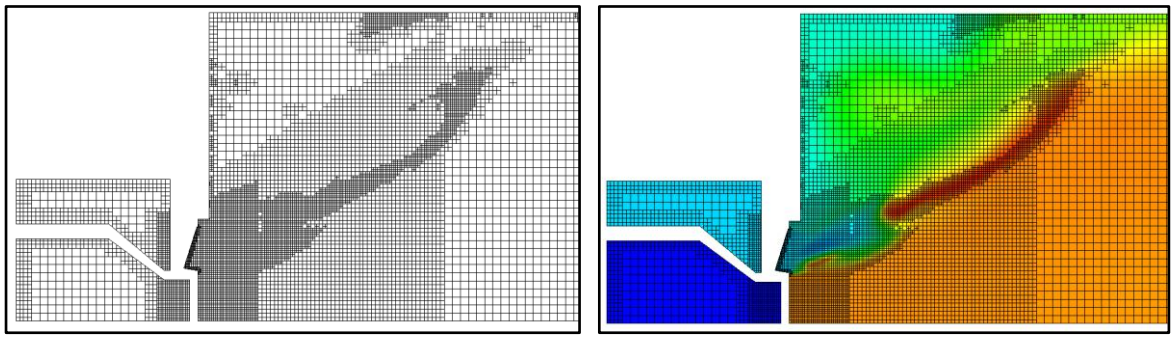

Figure 2: Adaptive mesh refinement for temperature in the recirculation zone

Turbulence Model

Turbulence significantly increases the rate of mixing of momentum, energy, and species. For a wide variety of applications, it is very difficult to obtain accurate CFD simulation results without including a turbulence model. Since it is not practical to resolve all length and time scales in a typical CFD simulation, turbulence models are used to account for the additional mixing and transport. The Reynolds Averaged Navier Stokes (RANS) equations with realizable $k-\varepsilon$ turbulence model is employed in the present study. The governing equations for RANS model in compressible form are shown below.

Conservation of Mass: $\frac{\partial \bar{\rho}}{\partial t}+\frac{\partial \bar{\rho}\widetilde{u_j}}{\partial x_j}=0$ (1)

Conservation of Momentum: $\frac{\partial \bar{\rho}\,\widetilde{u_i}}{\partial t}+\frac{\partial \bar{\rho}\widetilde{u_i}\widetilde{u_j}}{\partial x_j}=-\frac{\partial \bar{P}}{\partial x_i}+\frac{\partial}{\partial x_j}\left[\mu\left(\frac{\partial \widetilde{u_i}}{\partial x_j}+\frac{\partial \widetilde{u_j}}{\partial x_i}\right)-\frac{2}{3}\mu\frac{\partial \widetilde{u_k}}{\partial x_k}\,\delta_{ij}\right]-\frac{\partial \tau_{ij}}{\partial x_j}$ (2)

where $\tau_{ij}=-\bar{\rho}\widetilde{u_i'u_j'}$ is the Reynolds stress term resulting in the momentum equation due to ensemble averaging. The realizable $k-\varepsilon$ model is used for the RANS models to obtain closure for the above momentum equation. The realizable $k-\varepsilon$ model is chosen because it ensures the non-negativity of the turbulent normal stresses by imposing realizability constraints to satisfy the Schwartz′s inequality and this model works well for rotational flows. Turbulent viscosity is calculated as $\mu_t=C_\mu\rho\left(\frac{k^2}{\varepsilon}\right)$. Turbulent kinetic energy, k, and turbulent eddy dissipation, ε, are estimated by solving the following transport equations shown below,

$$\frac{\partial \bar{\rho}k}{\partial t}+\frac{\partial \bar{\rho}\widetilde{u_j}k}{\partial x_j}=\tau_{ij}\frac{\partial \widetilde{u_i}}{\partial x_j}+\frac{\partial}{\partial x_j}\left(\frac{\mu+\mu_t}{\mathrm{Pr_k}}\frac{\partial k}{\partial x_j}\right)-\rho\epsilon \quad (3)$$

$$\frac{\partial \bar{\rho}\varepsilon}{\partial t}+\frac{\partial \bar{\rho}\widetilde{u_j}\varepsilon}{\partial x_j}=\frac{\partial}{\partial x_j}\left[\left(\mu+\frac{\mu_t}{\sigma_\varepsilon}\right)\frac{\partial \varepsilon}{\partial x_j}\right]+C_1\rho\varepsilon\sqrt{S_{ij}S_{ij}}-C_2\rho\frac{\varepsilon^2}{k+\sqrt{\nu\varepsilon}}+C_{1\varepsilon}C_{3\varepsilon}P_b\frac{\varepsilon}{k} \quad (4)$$

Then C_μ is calculated as, $C_\mu=\frac{1}{A_0+A_s\frac{kU^*}{\varepsilon}}$, A_0 and A_s are model constants. U^* is friction velocity.

Detailed Chemistry

In the work, we compute the combustion reactions using the direct detailed chemistry solver (laminar finite rate chemistry). The detailed chemistry in the simulation is fully coupled with the fluid dynamics. Adaptive zoning of chemistry "bins" is not employed in the present study.

RESULTS AND DISCUSSION

We use a concept oxy-fuel combustor geometry created at SWRI by Delimont *et al* [11]. The geometry is experimental in nature and is part of the design study by SWRI, Thar Energy and others for creating a 1MW (thermal) sCO_2 combustor. The geometry looks similar to a traditional

gas fueled single axial combustor. This combustor has the key components envisioned for the final design, but the components are simplified in-order to facilitate a parametric design study. The combustor has three main zones: swirler, primary combustion and dilution. CO_2 captured from the exit is cycled back in the combustor through core inflow, effusion cooling holes and dilution holes. Core flow is composed of oxygen (obtained from air-separation unit upstream) premixed with super critical CO_2. The fuel, methane, is injected through circular holes along the inner diameter in the swirler. The remainder of bypass CO_2 is introduced in the combustor through effusion holes and two dilution slots halfway through the combustor. A schematic of the geometry is shown in Figure 3. In this work we use a quarter sector model with periodic faces for RANS simulations. We study two key topics of interest to the sCO_2 community: i) effect of mechanism on flame and CO prediction, ii) effect of CO addition at the inflow.

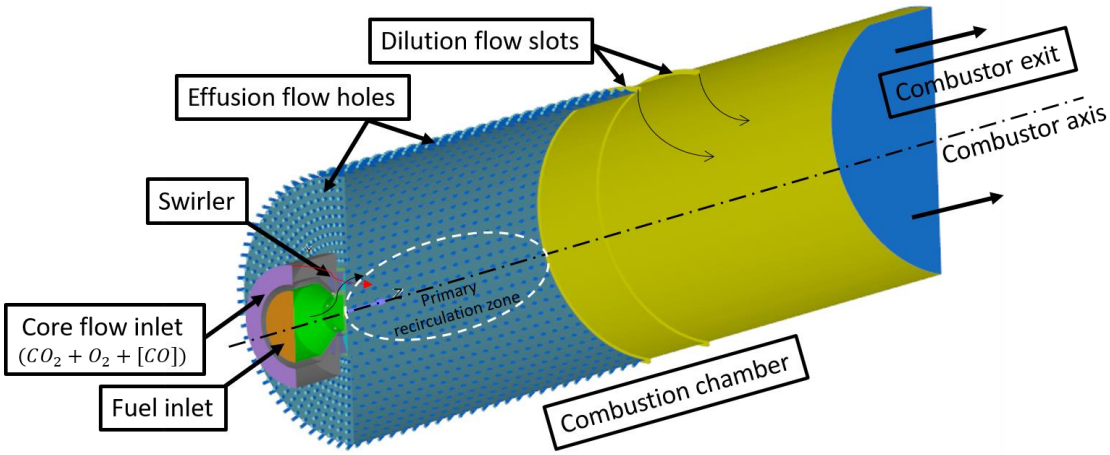

Figure 3: Schematic of SWRI concept combustor

Effect of Mechanism

We study two mechanisms widely used in the simulation community for methane combustion:

1. Cai-2017 (Cai, 2017) [14]: The mechanism was developed at RWTH Achen University (Germany) for oxy fuel combustion at high pressure (~30bar)
2. Saudi ARAMCO 2.0 (W.K. Metcalfe, 2013) [15]: The AramcoMech 2.0 builds upon AramcoMech1.3. It has been developed to characterize the kinetic and thermochemical properties of a large number of C1–C4-based hydrocarbon and oxygenated fuels. It was developed by the Combustion Chemistry Centre at NUI Galway (funded by Saudi Aramco). This mechanism has been validated for very high pressures. A reduced version of this mechanism (73 species) has been used in this work.

The goal is to qualitatively show the difference between the two mechanisms for methane combustion in prediction of flow, flame and emissions in the sCO_2 combustor. For this study we consider the case where no CO is added to the inflow stream. In Figure 4, the temperature and CO profile in the mid-plane of the concept sCO_2 combustor is plotted for simulations with two

different mechanisms (a) ARAMCO 2.0, and (b) Cai-2017. The two mechanisms give similar temperature and CO profile. There are some differences in the flame shape and the temperature in the corner recirculation zone, but overall, it concluded that both mechanisms perform equally well for sCO_2 combustion.

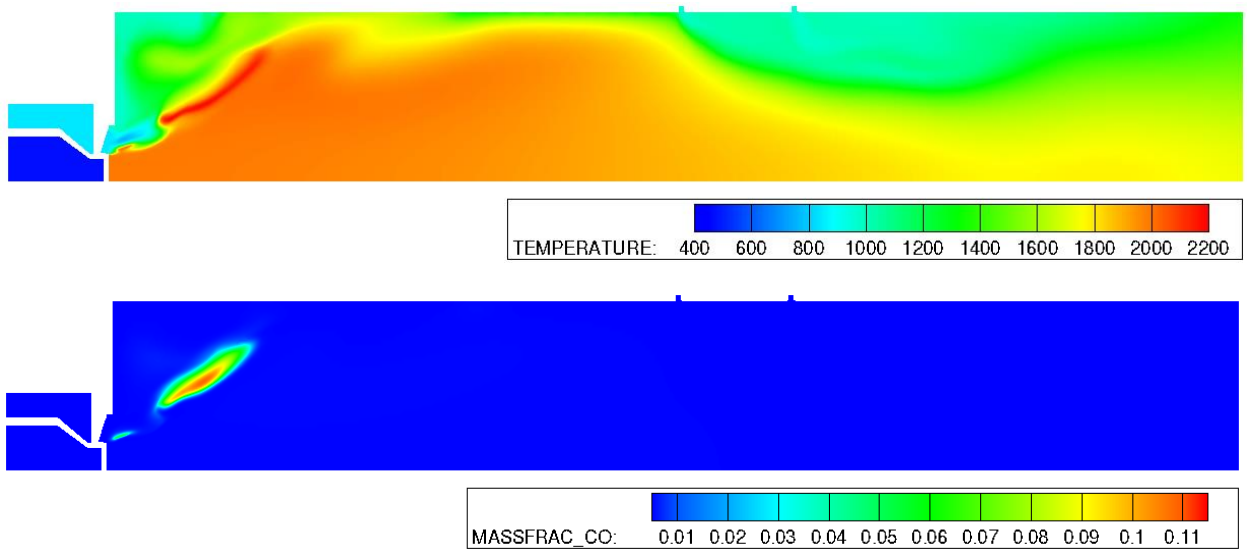

(a)

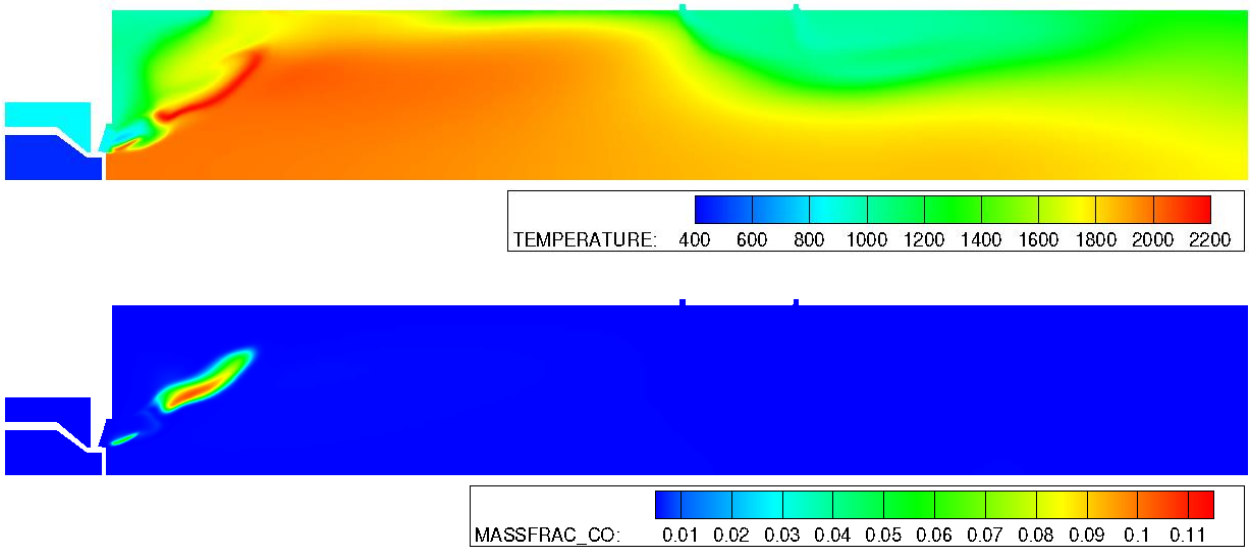

(b)

Figure 4: Temperature profile at the centerline plane of the sCO_2 combustor (a) ARAMCO 2.0, (b) Cai-2017

Effect of CO addition

sCO_2 combustors work in semi-closed loop, and the exhaust CO_2 is reintroduced in the combustion chamber after removing water and other impurities. Not all CO is removed and possibly a significant part of it makes its way back into the combustion chamber through mainstream, effusion, and dilution flow along with recycled CO_2. The loop can become unstable if positive feedback is established, wherein a small amount of CO in the inflow stream(s), increases the CO at outflow multiple fold. We investigate this problem using two approaches: 1) using a simplified model, a perfectly stirred reactor, 2) full 3D CFD modeling of the combustor.

Perfectly Stirred Reactor Model

The sCO_2 system is studied using a simplified model: a perfectly stirred reactor (PSR). The results would help understand the trend under various conditions. Table I below shows conditions for the PSR setup. We study three CO_2 dilution mass-fractions: $75\%, 90\%$ and 95%.

PSR inlet species	Flow rate
CH_4	$0.02\ kg/s$
O_2	$0.08\ kg/s$
CO_2	Varied between $75\%\ 90\%\ and\ 95\%$

Table 1: PSR inflow conditions

We first study the effect of residence time on exit CO. We consider the case with 75% CO_2 dilution and compute CO at the exit of PSR for two different residence times: $0.001s$ and $0.1s$, the latter being representative of a typical combustor residence time. In Figure 5, we see that the growth of CO is faster in the low residence time PSR reactor. This result is expected as in the case with low residence time there is not sufficient time available to oxidize CH_4 into CO_2. For the remainder of the study, we fix the residence time of PSR at $0.1s$.

Since our sCO_2 system works in a semi closed loop, CO at exit can find its way back into the combustor as exit CO_2 is recycled. This can potentially make the sCO_2 system unstable. We study the evolution of CO at exit using the PSR model. In each new cycle, we use the CO at the exit from the previous cycle. From Figure 6, we see that the concentration of CO increases in each cycle of operation for all three CO_2 dilution mass-fractions. The trend it not exponential, as suspected by some in the sCO_2 community. CO at the exit appears to settle down to a steady value in couple of cycles. In the case with 95% CO_2 dilution the reaction temperature is low and does not support complete conversion of CH_4 to CO_2, hence there is higher trace of CO. In the case with 75% CO_2 dilution the reaction temperature is up to $\approx 2300\ K$ and high-temperature pathways ($CH_4 \rightarrow CH_3 \rightarrow CO \rightarrow CO_2$) are prominent, therefore we observe higher trace of CO. The case with 90% CO_2 dilution sits close to the knee of the CO curve, where exit temperature is low but not low enough to substantially curb the full conversion of CH_4 to CO_2. The exit temperatures in different cycles are shown in Figure 7. As the CO_2 dilution mass fraction increases from 75% to 95% the exit temperature decreases overall. For each case, exit temperature shows a trend to reach

a steady value which is in-line with the trend in CO, as oxidation of CO is the major contributor to overall heat release.

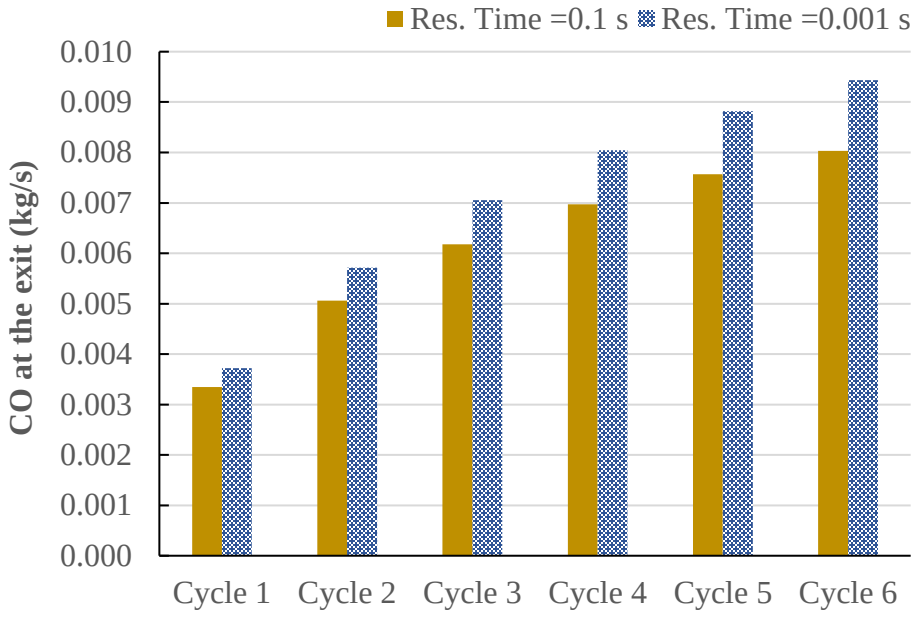

Figure 5: CO at PSR exit for different residence time cases

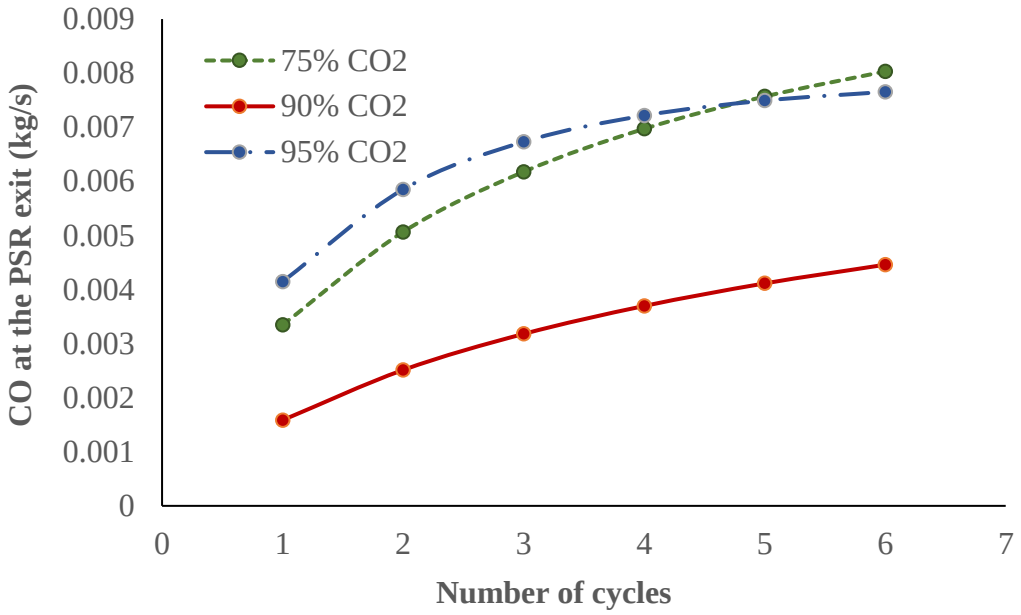

Figure 6: Evolution of exit CO in the PSR for different CO dilution cases. Each cycle uses the exit CO of the previous cycle as inflow condition for CO. Cycle 1 has no CO at inflow.

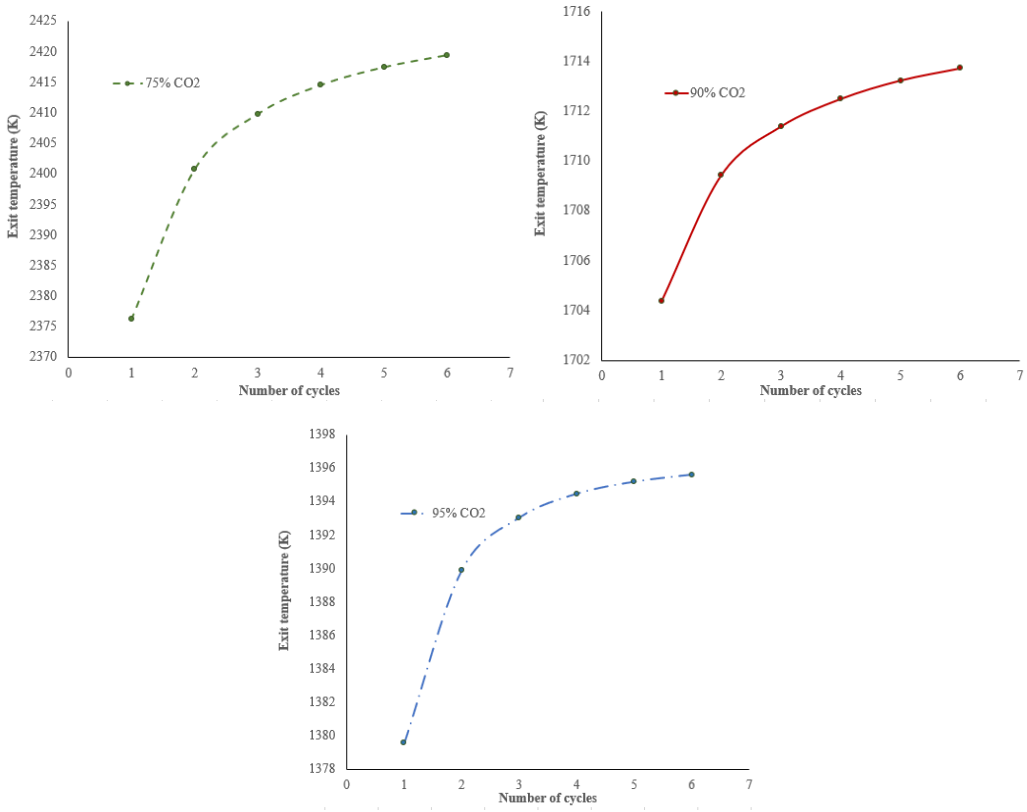

Figure 7: Evolution of exit temperature with cycles in different CO_2 dilution cases.

CFD Modeling

To investigate the effect of CO addition using full 3D CFD we simulate the reacting flow in the SWRI concept combustor using steady RANS and direct detailed chemistry. We study the combustor using both ARAMCO 2.0 and Cai-2017 mechanism. First, the combustor is run without any CO addition. The flux of CO and CO_2 mass fraction measured at the outflow is used to set the inflow mass fraction of CO and CO_2 for the next simulation. With CO from the $(N-1)^{th}$ round added to the inflow stream, N^{th} round simulation is performed and mass fraction of CO at the outflow is measured. If measured mass/mole fraction at outflow is higher than that introduced at the inflow, effusion or dilution jets combined, it would serve an indicator of a positive feedback.

	Outflow CO (kg/s)	
	ARAMCO 2.0	**Cai-2017**
Inflow CO = 0 kg/s	$1.6 \times 10^{-5}\ kg/s$	$1.6 \times 10^{-6}\ kg/s$
Inflow CO = $4.67 \times 10^{-5}\ kg/s$	$4.1 \times 10^{-5}\ kg/s$	$4.0 \times 10^{-5}\ kg/s$
Inflow CO = $6.1 \times 10^{-5}\ kg/s$	$4.5 \times 10^{-5}\ kg/s$	$4.6 \times 10^{-5}\ kg/s$

Table 2: Mass flux of CO (kg/s) at combustor outflow

	Outflow $X_{frac}(CO)/X_{frac}(CO_2)$	
	ARAMCO 2.0	**Cai-2017**
Inflow $X_{frac}(CO)/X_{frac}(CO_2) = 0$	7.6×10^{-5}	6.3×10^{-6}
Inflow $X_{frac}(CO)/X_{frac}(CO_2) = 1.9 \times 10^{-4}$	1.5×10^{-4}	1.6×10^{-4}
Inflow $X_{frac}(CO)/X_{frac}(CO_2) = 2.5 \times 10^{-4}$	1.9×10^{-4}	1.93×10^{-4}

Table 3: Ratio of mole fractions of CO to CO_2 at outflow

In Table 2, mass flux of CO computed at the exit of the combustor for different inflow CO mass flow rates (sum total of oxidizer, effusion and dilution streams) are tabulated. The results are also tabulated for two different mechanisms: ARAMCO 2.0, and Cai-2017. We see that as the mass flux of CO is increased in the inflow streams, CO at outflow (exit) increases too. The "delta" increase in outflow CO is less compared to what is added in the inflow. Also, we should remember that not all CO at the exit would be cycled back through inflow as some CO_2 (and some CO with it) is sequestered (or taken out for other applications like oil and gas). The above argument may be misleading as the amount of CO_2 at inflow and outflow are different due to the additional CO_2 added from combustion. Therefore, one should compare, for the inflow and outflow, the ratio of mole fraction of CO to CO_2. If the molar ratio of CO/CO_2 at outflow is smaller compared to that at the inflow, CO would continue to decrease with each cycle and eventually settle to a steady state value. Table 3 clearly shows that a positive feedback loop in CO would not be established which would otherwise adversely affect the performance of the sCO_2 system.

SUMMARY

In this work, we study two key mechanisms for methane combustion in sCO_2 combustors for prediction of flow, flame shape and emissions. We undertake a study to investigate the effect of CO addition and to determine whether a concept sCO_2 combustor would establish a positive feedback loop adversely affecting the performance of the combustion system. The concept combustor used for numerical study has been designed at SWRI. The numerical framework uses a direct detailed chemistry solver along with adaptive mesh refinement to capture the flame shape and flow gradients. The conclusions from this study are summarized below:

1. The two mechanisms studied, ARAMCO 2.0 and Cai-2017, show similar temperature and CO profile. The prediction of CO distribution is very similar between the two mechanisms.
2. *CO* addition to the inflow does not drive the sCO_2 combustor, working in a semi closed loop, into a positive feedback loop. Exit CO tends to reach an equilibrium value (PSR model) or reduce (3D CFD) compared to what is introduced at the inflow end.

Bibliography

[1] Allam, R., Fetvedt, J., Forrest, B., and Freed, D., "The oxy-fuel, supercritical CO_2 Allam Cycle: New cycle developments to produce even lower-cost electricity from fossil fuels without atmospheric emissions," Proc. ASME turbo expo 2014: turbine technical conference and exposition, American Society of Mechanical Engineers, pp. V03BT36A016-V003BT036A016.
[2] Vesely, L., Manikantachari, K. R. V., Vasu, S., Kapat, J., Dostal, V., and Martin, S., 2018, "Effect of Impurities on Compressor and Cooler in Supercritical CO_2 Cycles," Journal of Energy Resources Technology, 141(1), pp. 012003-012003-012008.
[3] Manikantachari, K. R. V., Martin, S., Bobren-Diaz, J. O., and Vasu, S., 2017, "Thermal and Transport Properties for the Simulation of Direct-Fired sCO_2 Combustor," Journal of Engineering for Gas Turbines and Power, 139(12).
[4] Manikantachari, K. R. V., Martin, S., Vesely, L., Bobren-Diaz, J. O., Vasu, S., and Kapat, J., "A Strategy of Reactant Mixing in Methane Direct-Fired sCO_2 Combustors," Proc. ASME Turbo Expo 2018: Turbomachinery Technical Conference and ExpositionV009T38A008.
[5] Manikantachari, K. R. V., Martin, S., Vesely, L., Bobren-Diaz, J. O., Vasu, S., and Kapat, J., "A Strategy of Mixture Preparation for Methane Direct-Fired sCO_2 Combustors," Proc. ASME Turbo Expo 2018: Turbomachinery Technical Conference and ExpositionV009T38A009.
[6] Manikantachari, K., Vesely, L., Martin, S., Bobren-Diaz, J. O., and Vasu, S., 2018, "Reduced Chemical Kinetic Mechanisms for Oxy/Methane Supercritical CO_2 Combustor Simulations," Journal of Energy Resources Technology, 140(9), p. 092202.
[7] Manikantachari, K. R. V., Martin, S., Rahman, R. K., Velez, C., and Vasu, S., 2019, "A General Study of Counterflow Diffusion Flames for Supercritical CO_2 Combustion," Journal of Engineering for Gas Turbines and Power, 141(12).
[8] Manikantachari, K. R. V., Martin, S., Rahman, R. K., Velez, C., and Vasu, S., "A General Study of Counterflow Diffusion Flames for Supercritical CO_2 Mixtures," Proc. ASME Turbo Expo 2019: Turbomachinery Technical Conference and ExpositionV04AT04A021.
[9] Portnoff, J. D. A. M. M., 2016, "Simulation of a Direct Fired Oxy-Fuel Combustion for sCO_2 Power Cycles," The 5th International Symposium- Supercritical CO_2 Power Cycles.
[10] Delimont, J., McClung, A., and Portnoff, M., "Direct Fired Oxy-Fuel Combustor for sCO_2 Power Cycles: 1MW Scale Design and Preliminary Bench Top Testing," Proc. ASME Turbo Expo 2017: Turbomachinery Technical Conference and ExpositionV009T38A027.
[11] Delimont, J., Andrews, N., and Chordia, L., "Computational Modeling of a 1MW Scale Combustor for a Direct Fired sCO_2 Power Cycle," Proc. ASME Turbo Expo 2018: Turbomachinery Technical Conference and ExpositionV009T38A025.
[12] Portnoff, J. D. A. M. M., "Simulation of a Direct Fired Oxy-Fuel Combustor for sCO_2 Power Cycles," The 5th International Symposium - Supercritical CO_2 Power Cycles, San Antonio, Texas.
[13] Strakey, P. A., 2019, "Oxy-Combustion Modeling for Direct-Fired Supercritical CO_2 Power Cycles," Journal of Energy Resources Technology, 141(7), p. 070706.
[14] Cai, L. S. (2017). Experimental design for discrimination of chemical kinetic models for oxy-methane combustion. Energy & Fuels, 5533-5542.
[15] W.K. Metcalfe, S. B. (2013). A hierarchical and comparative kinetic modeling study of C1–C2 hydrocarbon and oxygenated fuels. Int. Journal for Chemical Kinetics, 638–675.
[16] Richards, K.J., Senecal, P.K., and Pomraning, E., CONVERGE 2.4, Convergent Science, Madison, WI (2020).
[17] C.M Rhie, W. L. Chow “Numerical Study of the Turbulent Flow Past an Airfoil with Trailing Edge Separation,” AIAA J., vol. 21, no. 11, pp. 1525–1532, 1983.

[18] R. I. Issa, “Solution of the Implicitly Discretised Fluid Flow Equations by Operator-Splitting,” vol. 65, pp. 40–65, 1981.
[19] V. R. Hasti, P. Kundu, G. Kumar, S. A. Drennan, S. Som, and J. P. Gore, “Numerical Simulation of Flow Distribution in a Realistic Gas Turbine Combustor”, 2018 Joint Propulsion Conference (AIAA 2018-4956) (2018)
[20] V. R. Hasti, P. Kundu, G. Kumar, S. A. Drennan, S. Som, and J. P. Gore, “A Numerical Study of Flame Characteristics during Lean Blow-Out in a Gas Turbine Combustor”, 2018 Joint Propulsion Conference
[21] E. Pomraning, “Development of Large Eddy Simulation Turbulence Models,” University of Wisconsin-Madison, Madison, WI, 2000